Chemical Papers (2022) 76:7295–7303
https://doi.org/10.1007/s11696-022-02410-x

ORIGINAL PAPER

Facile synthesis of magnetic porous carbon nanosheets as efficient As(III) adsorbent

Yiwei Luo[1] · Zeliang Wu[2] · Qihui Guan[2] · Shixia Chen[2] · Daishe Wu[1,3]

Received: 8 March 2022 / Accepted: 2 August 2022 / Published online: 13 August 2022

Abstract

Herein, magnetically modified biomass camphor seeds husk (MBC) was developed as an efficient biosorbent for remediation of arsenite (As(III))-polluted wastewater. The results of the SEM + EDS, TEM, XRD, and BET demonstrate the as-obtained adsorbents were Fe species impregnated amorphous porous carbon nanosheets. The effects of adsorbent dosage, solution pH, contact time, initial concentration, and co-existing ions were systemically investigated. As a result, the MBC delivers a maximum adsorption capacity of 39.7 mg/g based on the Langmuir model at natural pH. Moreover, the MBC could also maintain superior As(III) removal performance in wide pH values ranging from 5 to 10. And the commonly coexisting anions showed slight effect on the As(III) removal. FT-IR and XPS of the MBC before and after As(III) adsorption revealed the removal mechanism was dominated by the surface complexation, oxidation, and H-bonds.

Keywords Biosorbent · Carbon nanosheets · Arsenite · Fe_3O_4

Introduction

Rapid urbanization and industrialization inevitably induce the release of toxic metals into the water. Among these, arsenic (As) pollution is deemed as a potential environmental and public health issue to human beings due to its threat of high toxicity, non-biodegradation, and accumulation through the food chain(Zhu et al. 2016). The accumulation of As in groundwater is mainly from the weathering of As-rich minerals and poorly disposed of metallurgical, mining industries, and As-containing pesticides. Intaking of As could cause serious diseases to human beings, such as skin, lung, bladder, and kidney cancer. Arsenite (As(III)) and arsenate (As(V)) are commonly existing inorganic As species, and As(III) dominates as the H_3AsO_3 species while As(V) appears as a mixture of the H_2AsO^{4-} and $HAsO_4^{2-}$ species with normal pH range from 4 to 8. As previously reported, As(III) is 60-folds more toxic and mobile than As(V) (Shakoor et al. 2019; Amen et al. 2020). Thus, developing an efficient strategy for the remediation of As(III))-contaminated water is urgently needed.

To date, various technologies such as chemical precipitation, ion exchange, electrochemical techniques, and membrane separation have emerged to tackle the As-contaminated water (Samuel et al. 2021; Alka et al. 2021). However, adsorption is still considered one of the most promising processes owing to its low cost, high efficiency, and facile operation (Cheng et al. 2021; Luo et al. 2021; Han et al. 2022). Till now, kinds of novel materials such as activated carbon (Budinova et al. 2006), layered double hydroxides (Li et al. 2021), porous metal–organic frameworks(MOFs) (Wang et al. 2019), industrial byproducts, and wastes (Rha and Jo 2021), have been used as As(III) adsorbents. Nevertheless, most of the adsorbents are pH-sensitive in As(III)-containing solution due to the protonation of functional groups on the adsorbent surface and the speciation of As in the aqueous medium (Samuel et al. 2021). To this end, an additional pH modifier is inevitable which will increase the cost in

Yiwei Luo and Zeliang Wu are equally contributed to this work.

✉ Shixia Chen
shixiachen@ncu.edu.cn

✉ Daishe Wu
dswu@ncu.edu.cn

[1] School of Resource and Environment, Nanchang University, Nanchang 330031, Jiangxi, People's Republic of China

[2] School of Chemistry and Chemical Engineering, Nanchang University, Nanchang 330031, Jiangxi, People's Republic of China

[3] School of Materials and Chemical Engineering, Pingxiang University, Pingxiang 337000, People's Republic of China

practical application. Thus, developing a more economical and facile adsorbent is still challenging.

Biomass possesses great application prospects in the treatment of water pollution issues due to its environmentally benign, low cost, and tunable surface properties (Chen et al. 2018a, b; Chen et al. 2018a, b) (Chen et al. 2020a, b). Seed husks are reported as effective biosorbents to remove anionic and cationic heavy metals from aqueous solutions (Ullah et al. 2020; Somasekhara Reddy et al. 2017). *Cinnamomum camphora* is an evergreen broad-leaved tree species extensively distributed in south China. And the seeds are usually applied to extract the oil, hereafter the seed husks are thrown away which might be washed to the river by the rain or burned outside and cause a threat to the environment (Liu et al. 2018). Conversion of biomass to biochar is an efficient way to construct biosorbent but is still hindered by the limited adsorption sites, which failed to achieve satisfactory pollution removal performance (Qin et al. 2020). Magnetically modified biochar not only displays a strong affinity to As(III) but is easy to be recycled, which has been considered as one of the most promising functionalized strategies (Tabatabaiee Bafrooee et al. 2021; Li et al. 2020; Zhang et al. 2019). In addition, the introduction of iron speciation will improve the removal process via surface complexation and oxidation, which weaken the effect of pH (Amen et al. 2020). To the best of our knowledge, the spent camphor seeds husk (CSH) derived magnetic biochar has not been examined on the As(III) removal yet.

Herein, a facile one-step calcination method is developed to construct the magnetic biomass-derived carbon nanosheets (MBC) as efficient As(III) adsorbents. Spent CSH was applied as feedstocks, and $FeCl_3$ was adopted as Fe sources. Then, the $FeCl_3$ pretreated CSH was annealed under N_2 atmospheres at 700 °C for 2 h. The as-obtained MBC yields a superior adsorption capacity of 39.7 mg/g based on a Langmuir model at natural pH and quick adsorption equilibrium time within 120 min. In addition, the adsorbent could also be efficient in a wide pH range from 5 to 10 and possessed a slight effect by the coexisting ions. This work provides a theoretical reference for the high-value utilization of biowaste and the effective treatment of As(III) in wastewater.

Experiment section

Chemicals and raw materials

All the reagents used in this work were analytical grade and employed as purchased without further purification. Camphor seeds husk (CSH), obtained from the spent *Cinnamomum camphora* seeds from Jiangxi Province Key Laboratory of Edible and Medicinal Resources Exploitation of Nanchang University, were dried overnight at 80 °C in an oven then chopped with a mechanic mill and sieved to particle sizes below 0.45 mm for subsequent experiments.

Preparation of magnetic biomass-derived carbon nanosheets (MBC)

For the synthesis of MBC, a one-step calcination method was applied. Typically, the spent CSH powder (10 g) was immersed in 50 mL $FeCl_3$ solution ($FeCl_3$/CSH ratio = 0.1), and stirring at 80 °C for 120 min for vaporization of water. Subsequently, the Fe-impregnated sample was transferred to the tubular reactor and started at 200 °C under N_2 with a flow of 500 mL/min for 1 h, then the temperature was raised to 700 °C under heating rate of 10 °C/ min, and maintained for 2 h. After cooling naturally, the sample was washed thoroughly with deionized water and dried overnight to obtain the MBC. For comparison, the BC was prepared without the addition of $FeCl_3$.

Characterization

The morphology and microstructure were observed on scanning electron microscopy (SEM, FEI Nova Nano SEM450, Czech) and transmission electron microscopic (TEM, Talos F200X, Netherlands). The structural properties were revealed by the powder X-ray diffraction (XRD, PANalytical empyrean series2, Netherlands) with Cu-Kα radiation at room temperature from 5 to 90 °C and Raman microscopy (HORIBA Jobin Yvon, France) with 532 nm radiation. The changes of the surface chemical composition and functional groups were disclosed by the Fourier Transform Infrared spectrometer (FT-IR, Nicolet, America) from 400 to 4000 cm^{-1} and X-ray photoelectron spectroscopy (XPS, Axis Ultra DLD, Japan). The magnetic properties of the samples were measured with a Lakeshore7404 vibrating sample magnetometer (VSM).

Batch adsorption experiments

The batch adsorption experiments were conducted in a temperature-controlled shaker with a rotation speed of 160 rpm. The effect of dosage was conducted by adding the adsorbent amount of 15, 30, 60, 120, and 150 mg to 30 mL solutions under natural pH for 8 h, respectively. Then, 30 mg of the adsorbent was added to 30 mL solutions with different pH values, different contact times, and different initial concentrations. The pH values were adjusted by using 0.1 M HCl or NaOH. The contact time was set from 5 to 720 min for the kinetic experiment. The initial concentration was set from 10 to 100 mg/L. The coexisting anions of Cl^-, NO_3^-, SO_4^{2-}, HCO_3^-, and CO_3^{2-} were prepared from their corresponding sodium salts. After adsorption, the suspension

was immediately filtered with a 0.22 μm microfiltration membrane. And the concentration of As was quantified by an atomic fluorescence spectrometer (AFS-8220, Beijing Haitian Instruments, China).

Results and discussion

Characterization of the adsorbents

Scanning electron microscope (SEM) and transmission electron microscopic (TEM) were used to disclose the morphology change of the biomass-derived carbon after magnetic modification. As displayed in Fig. 1a, b, and c, the unmodified BC was large and thick chunks with a smooth surface. Upon $FeCl_3$ treatment, the magnetic MBC were shown as thin carbon nanosheets with rough surfaces (Fig. 1d, e, and f). This might be due to the activation of the $FeCl_3$, which could endow a larger surface area on MBC and boost the As(III) immobilization(Cho et al. 2017). The high-resolution TEM (HRTEM) image indicates the poor crystallinity and amorphous carbon structure of MBC (Fig. S1) while the energy dispersive X-ray spectroscopy (EDS) spectra suggests the successful impregnation of Fe species (Fig. S2). Moreover, the corresponding EDS mapping images suggests the element of C, O, and Fe are evenly distributed on the MBC (Fig. 1g).

The structural properties of the obtained biochar with and without treatment of $FeCl_3$ were revealed by the XRD. As depicted in Fig. 2a, the diffraction peak at about 22.5 °C for both samples can be assigned to the reflection of graphite (002) (JCPDS: No. 41–1487). And the broad and low-intensity (002) diffraction peak imply the amorphous character of the obtained adsorbents (Chen et al. 2018a, b). The newly emerged characteristic peaks at $2\theta = 35.5°$, 43.1°, 57.0°, and 62.6° were related to the planes of (311), (400), (511) and (440) of the cubic Fe_3O_4 (JCPDS 88–0866), suggesting the loaded Fe oxide in MBC was identified mainly as magnetite (Fe_3O_4) (Zhang et al. 2020a, b). The Fe_3O_4 could maintain MBC with superior magnetism, as revealed in Fig. 2b. Raman spectra were further applied to investigate the graphitization degree and defects. As illustrated in Fig. 2c, both samples displayed an obvious D band at 1343 cm^{-1} and G band at 1580 cm^{-1}, which can be assigned to the disordered and graphite structures of carbon, respectively (Jiang et al. 2019). It can be seen that the intensity ratio values of I_D/I_G increased from 0.875 to 0.955 on MBC, indicating more defect sites in MBC (Kolagatla et al. 2018), which was consistent with the SEM results. The mass loading of the Fe is calculated to be about 10.35% based on the XPS results (Table S1). And the carbon content decreased from 77.3% of BC to 66.0% of MBC due to the impregnated Fe species (Table S2). Moreover, the N_2 adsorption–desorption

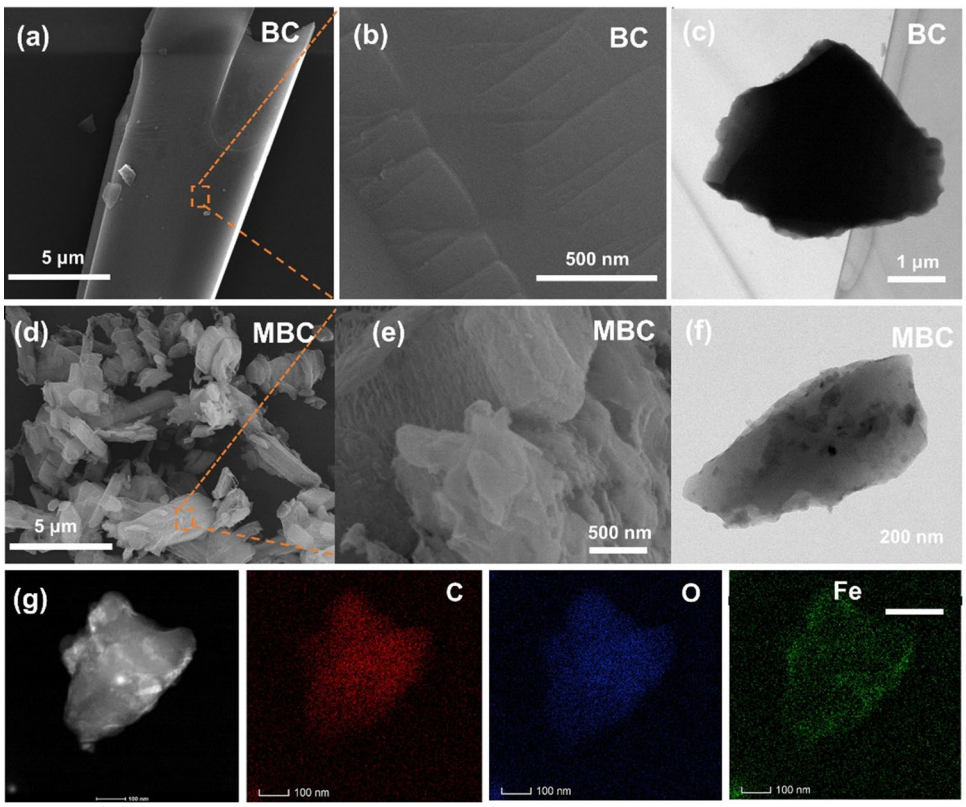

Fig. 1 SEM images of **a** BC and **b** enlarged BC surface, **c** TEM images of BC; SEM images of **d** MBC and **e** enlarged MBC surface, **f** TEM images of MBC, and **g** corresponding EDS mapping images

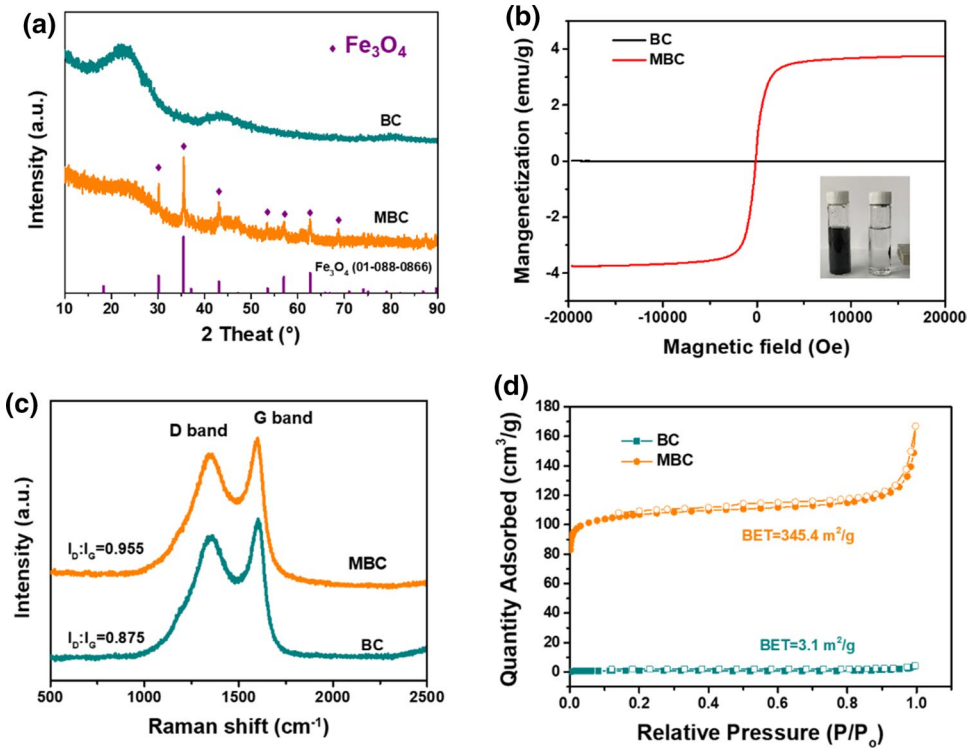

Fig. 2 **a** XRD pattern, **b** Magnetic hysteresis loop, **c** Raman spectra, and **d** N_2 adsorption–desorption isotherms at 77 K of BC and MBC

isotherms were measured at 77 K to investigate the $FeCl_3$ treatment on the surface properties of biochar. As illustrated in Fig. 2d, both BC and MBC exhibited type IV isotherm with type H4 hysteresis according to the IUPAC classification, implying the mesoporous carbon materials (Chen et al. 2018a, b). The calculated BET surface area of MBC is 345.4 m^2/g, which was much higher than the BC (3.1 m^2/g). This might be due to the activation of the $FeCl_3$ and the formation of Fe_3O_4 during the reaction, suggesting the simultaneous activation and magnetization on MBC by $FeCl_3$ treatment (Zhang et al. 2020a, b). The large surface area could render MBC with highly accessible As(III) sites thereby affording high As(III) capacity.

As(III) adsorption performance

Effect of dosage and pH

The effect of the dosage of the MBC on As(III) adsorption was investigated. As shown in Fig. 3a, the removal efficiency increased with the increasing dosage, when the dosage was raised to 5 g/L, the removal efficiency can achieve above

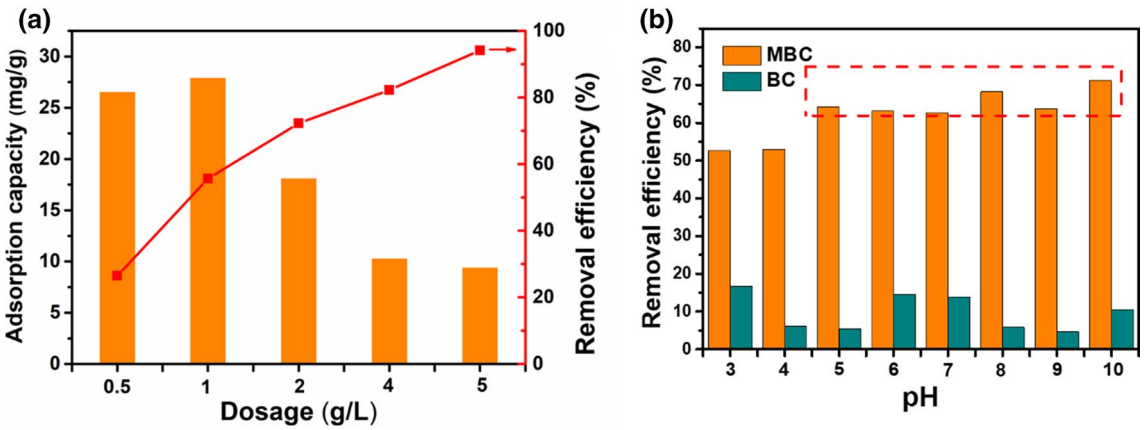

Fig. 3 **a** Effect of the dosage and on the MBC for As(III) adsorption capacity and removal efficiency, **b** Effect of pH on the BC and MBC for As(III) adsorption capacity. Initial concentration = 50 and 20 mg/L for dosage and pH effect, respectively, pH = natural, adsorbent dose = 1 g/L

95%. However, the adsorption capacity q_e reach the maximum of 28.0 mg/g at 1 g/L, and then declined with the increase of adsorbent dosages. This might be due to the limited adsorption sites at a lower dosage and overlapped binding sites at the higher dosage (Zhang et al. 2021). So, 1 g/L dosage was applied for further experiment. pH values play a vital role in the adsorption because it affects the charge state of the pollution and adsorbent (Tang et al. 2019a, b; Tang et al. 2019a, b). As displayed in Fig. 3b, As(III) adsorption of MBC had the highest removal efficiency (above 62%) at a wide pH range from 5 to 10, which satisfies the pH range of 6–8.5 in groundwater. However, for BC, the As(III) removal efficiency is highly pH-dependent. In general, As(III) exists in the form of $H_3AsO_3^0$ at < pH 9, and $H_2AsO_3^-$ at pH 9–11 (Rha and Jo 2021). So the increase of the As(III) removal efficiency above pH 9 is due to the electrostatic attraction between arsenic ions and the charged material surfaces. The much higher As(III) removal efficiency on MBC than BC in a wide pH range manifests the dominated As(III) immobilization mechanism is caused by the effect of iron species. Because the natural pH in As(III) solution is about 7.2, to avoid the cost of an additional pH modifier, a natural pH value was adopted in the further experiment.

Adsorption kinetics and isotherms

The adsorption kinetics of As(III) by BC and MBC are depicted in Fig. 4a. Both BC and MBC showed quick equilibrium on As(III) sorption within 2 h and exhibited only a slight increase hereafter. Obviously, MBC exhibited much higher capacities than that of BC all over the reaction time from 5 to 720 min. The nonlinear fitting curves of pseudo-first- and pseudo-second-order models were presented in Fig. 4a and the calculated fitting parameters were shown in Table 1. The correlation coefficients R^2 (0.950 and 0.987, respectively) of the pseudo-second-order model were higher than that of the pseudo-first-order model, suggesting the pseudo-second-order model was more consistent with As (III) adsorption by both BC and MBC. This also implies the adsorption process was mainly controlled by the amount of the active sites on their surface. To achieve complete adsorption, the reaction time was set as 8 h.

Table 1 Adsorption kinetic models and parameters for removal of As (III) on BC and MBC

Parameters	BC	MBC
Pseudo-first-order		
q_e (mg/g)	13.68	34.12
k_1 (min^{-1})	0.1223	0.0549
R^2	0.907	0.968
Pseudo-second-order		
q_e (mg/g)	14.30	36.40
k_2 (g/(mg·min))	0.0131	0.0023
R^2	0.950	0.987

To disclose the adsorption mode on the as-obtained MBC and evaluate the maximum adsorption capacity. The adsorption isotherm experiments were carried out with initial As (III) concentrations ranging from 10 to 100 mg/L for 8 h. As illustrated in Fig. 4b, the capacity q_e of both BC and MBC increased quickly in the low concentrations and tend to equilibrium at high concentrations. The nonlinear fitting curves of Langmuir and Freundlich models were presented in Fig. 4b and the obtained relevant parameters were listed in Table 2. The higher R^2 for the Langmuir model on BC (0.853) and MBC (0.994) demonstrate the adsorption behavior of As(III) on both BC and MBC were in better pertinence with the Langmuir model. This result suggests the chemisorption on the surface of the adsorbents. And

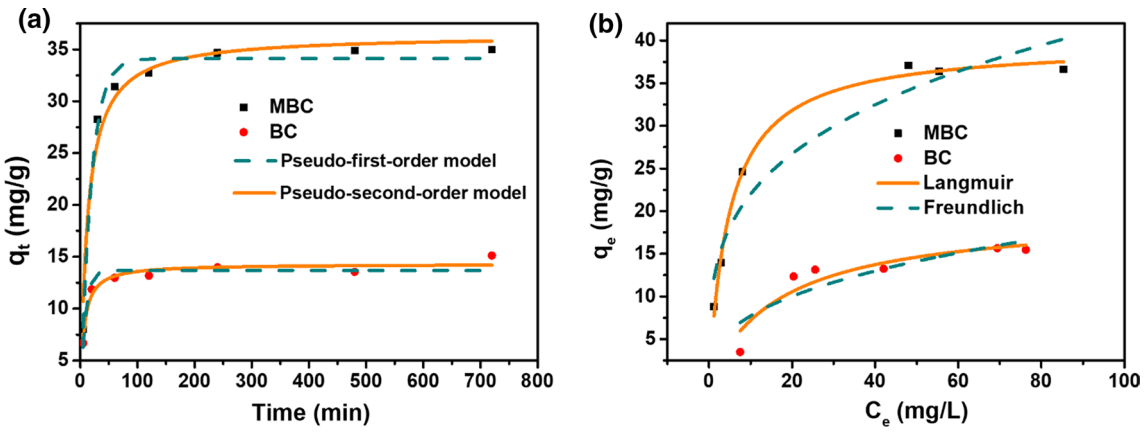

Fig. 4 **a** Nonlinear fittings of adsorption kinetics using pseudo-first-order and pseudo-second-order models, initial concentration = 50 mg/L, pH = natural, adsorbent dose = 1 g/L; and **b** nonlinear fittings of adsorption isotherms using Langmuir and Freundlich models, pH = natural, adsorbent dose = 1 g/L, contact time = 8 h

Table 2 Adsorption equilibrium models and parameters for removal of As (III) on BC and MBC

Parameters	BC	MBC
Langmuir		
q_m (mg/g)	19.6	39.7
K_L(L/mg)	0.123	0.202
R^2	0.853	0.994
Freundlich		
K_F(mg^{1-n} L^n/g)	3.27	12.6
1/n	0.374	0.281
R^2	0.715	0.920

the calculated maximum adsorption capacity on MBC is 39.7 mg/g, about twofold higher than that of BC (19.6 mg/g). The removal performance outperforms most of the recently reported literature (Table 3).

Effect of coexisting ions

To evaluate the application of MBC in real water systems, the effect of some common co-existing anions (Cl^-, NO_3^-, SO_4^{2-}, HCO_3^- and CO_3^{2-}) on the As(III) adsorption was investigated. The adsorption retention represents ratio of the adsorption capacity of As(III) under different co-existing anions to that under blank solution without co-existing anion. As observed in Fig. 5a, the adsorption capacity of As(III) by BC was obviously affected by the co-existing anions. The maximum As(III) capacity decrease was affected by SO_4^{2-} and the adsorption retention only remained 3.7% at the concentration of 1.0 mg/L SO_4^{2-}. And the adsorption effect for coexisting ions of As(III) by BC is following $SO_4^{2-} > HCO_3^- > CO_3^{2-} > Cl^- > NO_3^-$. Conversely, the adsorption capacity of As(III) by MBC was slightly affected by the co-existing anions. As shown in Fig. 5b, even when the concentrations of the co-existing anions increased from 0.1 to 1.0 mg/L, the q_e of As(III) on MBC decreased less than 17%. This also proves that the As(III) adsorption properties on MBC were rarely relevant with the charge state of the pollution, which was consistent with the pH effect results.

Table 3 As(III) adsorption performance compared with other literatures

Sample	Initial concentration range (mg/L)	Dosage (g/L)	pH	Adsorption capacity(mg/g)	Refs.
Fe–Mn-La-BC	10–80	1	7	15.3	(Lin et al. 2019)
Waste foundry dust (WFD)	1–100	2.5	3	12.6	(Rha and Jo 2021)
Bi-BC	5–200	2	9.3	16.2	(Zhu et al. 2016)
Bacillus thuringiensis strain WS3 biomass	3–7	0.5	7	10.9	(Altowayti et al. 2019)
H-CAFBs	0.1–50	1	7	24.1	(Zeng et al. 2020)
Bark-based magnetic iron oxide particle (BMIOP)	0.092–1.981	1	7	19.6	(Dhoble et al. 2018)
BC	10–100	1	Natural	19.6	This work
MBC	10–100	1	Natural	39.7	

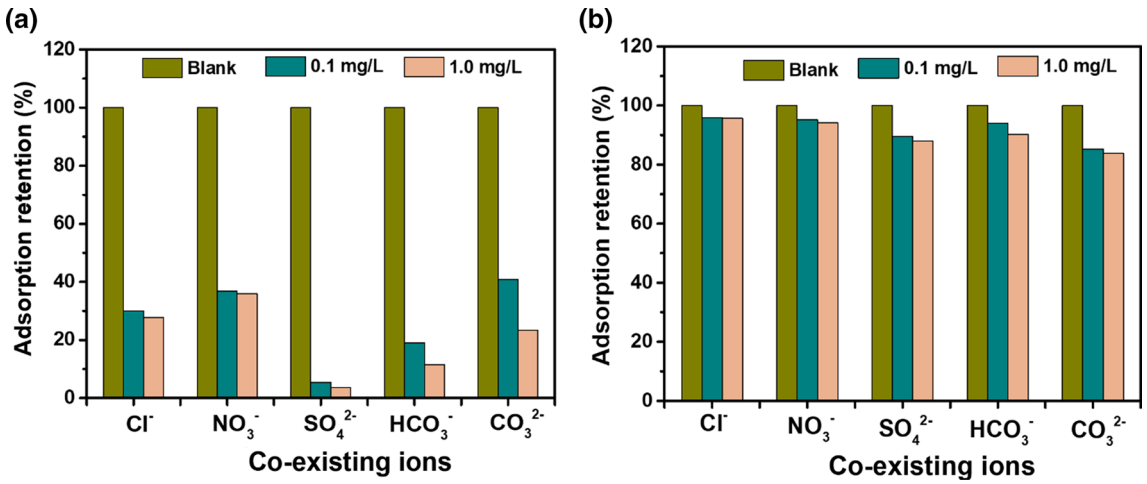

Fig. 5 Effect of co-existing ions on As(III) removal by **a** BC and **b** MBC. Initial concentration = 20 mg/L, pH = natural, adsorbent dose = 1 g/L

Adsorption mechanism

In order to explicate the possible mechanism of As(III) removal onto MBC, FTIR and X-ray photoelectron spectroscopy (XPS) were carried out on the adsorbent before and after the As(III) immobilization. As shown in Fig. 6a, a large number of functional groups appeared on the surface of MBC. The peaks detected at 3386 cm^{-1}, 2358 cm^{-1}, 1576 cm^{-1}, 1410 cm^{-1}, and 1088 cm^{-1} can be assigned to the stretching vibration of -OH, $-CH_3$, -C = O, -O = CO-, and C–OH bonds (Wen et al. 2017; Meng et al. 2021). And the peaks between 500 and 900 cm^{-1} were mainly ascribed to the Fe–O bond (Rha and Jo 2021). Upon As(III) adsorption, the obvious shifts of the O-containing groups and Fe–O bond indicate the participation of these functional groups in the removal of As(III) through complexation (Amen et al. 2020; Cuong et al. 2021). XPS survey spectrum of fresh MBC and As-MBC demonstrate the successfully adsorption of As (Fig. S3), and the spectrum of C1s, Fe 2p, and As 3d was deeply investigated to disclose the removal detail. As depicted in Fig. 6b, the C 1 s derived from the biochar could be deconvoluted into four characteristic peaks attributed to C–C (284.8 eV), C-O (285.5 eV), C = O (286.7 eV), and O = C–O (289.1 eV) (Gong et al. 2017; S. Chen et al. 2020a, b). The ~ 0.2% and ~ 1.5% decrease of C-O and C = O peaks implies the C–O and C = O functional groups could aid the immobilization of the As(III) onto the adsorbent surface through H-bond formation (Amen et al. 2020). As shown in Fig. 6c, the Fe $2p_{3/2}$ spectrum can be resolved into Fe(II) oxide peaks at 711.2 eV, an Fe(III) oxide peak at 713.2 eV. The ~ 2.4% increase proportion of Fe(III) after As(III) adsorption was most probably resulted from the oxidative transformation of Fe_3O_4 to Fe_2O_3 by dissolved O_2 in the reaction system during agitation (Zhang et al. 2016). The adsorbed As on the MBC are mainly existed as As(III) (83.4%) and As(V) (16.6%), which proved part of As(III) adsorption was the oxidative transformation caused by the Fe_3O_4 (Fig. 6d). In summary, the possible removal mechanisms of As(III) include surface complexation, oxidation, and H-bonds (Fig. 7). Moreover, the unique large surface area from the as-obtained MBC could also provide highly accessible As(III) sites thereby affording high As(III) capacity.

Conclusions

Spent camphor seeds husk (CSH)-based magnetic porous carbon (MBC) was successfully prepared by pyrolysis of $FeCl_3$ pretreated CSH. And simultaneous activation and magnetization were obtained on the MBC. As a result, the MBC possesses a variety of functional groups, which enhance the As(III) removal through surface complexation, oxidation, and H-bonds. Thus, the MBC can achieve

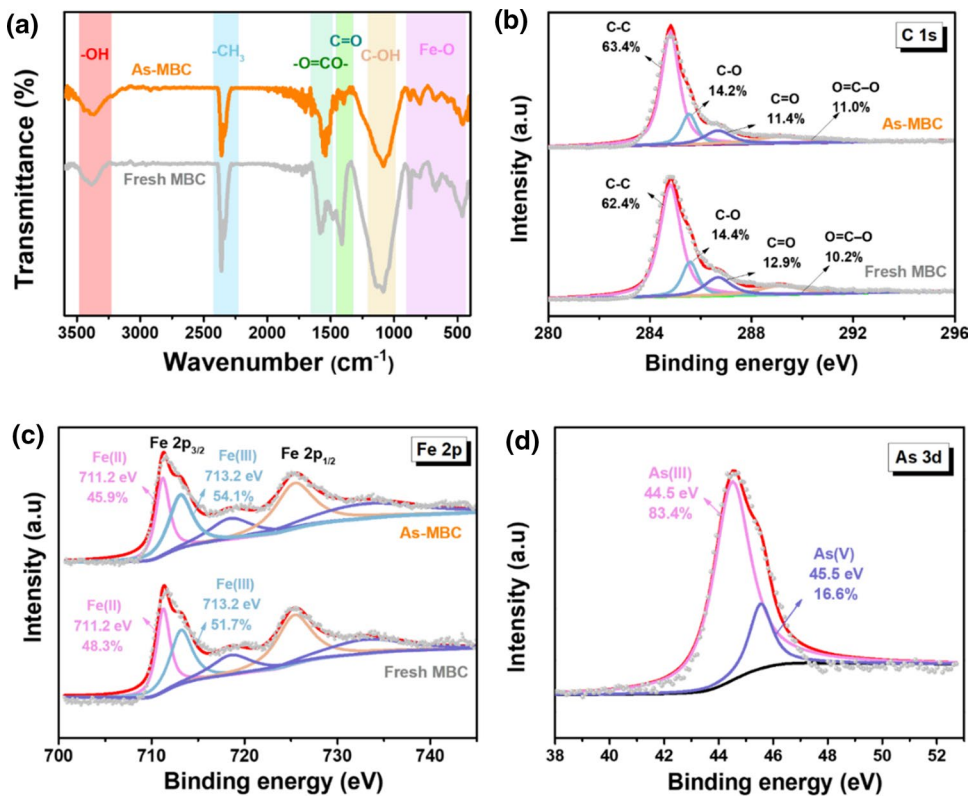

Fig. 6 **a** FT-IR spectra and **b** C1s XPS spectra, **c** Fe 2p XPS spectra, and **d** As 3d XPS spectra of Ni/Al@PAB before and after adsorption of As(III)

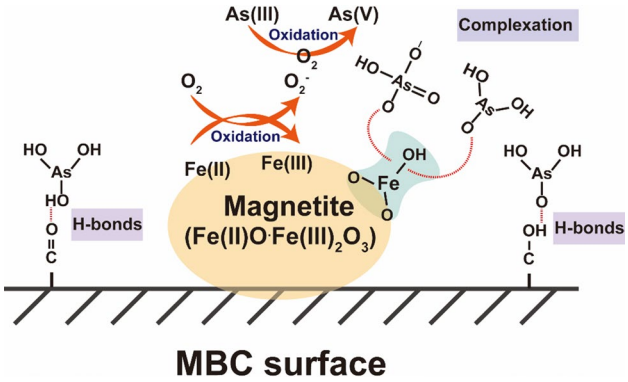

Fig. 7 Possible mechanisms for the immobilization of As on MBC

a maximum adsorption capacity of 39.7 mg/g based on the Langmuir model at natural pH, almost twofold higher than that of BC (19.6 mg/g). Moreover, the MBC could also maintain excellent As(III) adsorption during wide pH values from 5 to 10.

Supplementary Information The online version contains supplementary material available at https://doi.org/10.1007/s11696-022-02410-x.

Acknowledgements This research work was supported by the National Natural Science Foundation of China (No. 22008101) and the Natural Science Foundation of Jiangxi Province (No. 20212BAB213038).

Declarations

Conflict of interest The authors declare no competing financial interest.

References

Alka S, Shahir S, Ibrahim N, Ndejiko MJ, Vo DVN, Manan FA (2021) Arsenic removal technologies and future trends: a mini review. J Clean Prod 278:123805

Altowayti WAH, Algaifi HA, Bakar SA, Shahir S (2019) The adsorptive removal of As (III) using biomass of arsenic resistant Bacillus thuringiensis strain WS3: characteristics and modelling studies. Ecotoxicol Environ Saf 172:176–185

Amen R, Bashir H, Bibi I, Shaheen SM, Niazi NK, Shahid M et al (2020) A critical review on arsenic removal from water using biochar-based sorbents: The significance of modification and redox reactions. Chem Eng J 396:125195

Budinova T, Petrov N, Razvigorova M, Parra J, Galiatsatou P (2006) Removal of arsenic(III) from aqueous solution by activated carbons prepared from solvent extracted olive pulp and olive stones. Ind Eng Chem Res 45(6):1896–1901

Chen S, Huang Y, Han X, Wu Z, Lai C, Wang J et al (2018a) Simultaneous and efficient removal of Cr(VI) and methyl orange on LDHs decorated porous carbons. Chem Eng J 352:306–315

Chen S, Wang J, Wu Z, Deng Q, Tu W, Dai G et al (2018b) Enhanced Cr(VI) removal by polyethylenimine- and phosphorus-codoped hierarchical porous carbons. J Colloid Interface Sci 523:110–120

Chen Q, Tan X, Liu Y, Liu S, Li M, Gu Y et al (2020a) Biomass-derived porous graphitic carbon materials for energy and environmental applications. J Mater Chem A 8(12):5773–5811

Chen S, Lu C, Liu L, Xu M, Wang J, Deng Q et al (2020b) A hierarchical glucose-intercalated NiMn-G-LDH@$NiCo_2S_4$ core-shell structure as a binder-free electrode for flexible all-solid-state asymmetric supercapacitors. Nanoscale 12(3):1852–1863

Cheng N, Wang B, Wu P, Lee X, Xing Y, Chen M, Gao B (2021) Adsorption of emerging contaminants from water and wastewater by modified biochar: a review. Environ Pollut 273:116448

Cho DW, Yoon K, Kwon EE, Biswas JK, Song H (2017) Fabrication of magnetic biochar as a treatment medium for As(V) via pyrolysis of $FeCl_3$-pretreated spent coffee ground. Environ Pollut 229:942–949

Cuong DV, Wu PC, Chen LI, Hou CH (2021) Active MnO_2/biochar composite for efficient As(III) removal: Insight into the mechanisms of redox transformation and adsorption. Water Res 188:116495

Dhoble RM, Maddigapu PR, Bhole AG, Rayalu S (2018) Development of bark-based magnetic iron oxide particle (BMIOP), a bio-adsorbent for removal of arsenic (III) from water. Environ Sci Pollut Res 25(20):19657–19674

Gong Y, Li D, Luo C, Fu Q, Pan C (2017) Highly porous graphitic biomass carbon as advanced electrode materials for supercapacitors. Green Chem 19(17):4132–4140

Han YS, Kim SH, Jang JY, Ji S (2022) Arsenic removal characteristics of natural Mn-Fe binary coating on waste filter sand from a water treatment facility. Environ Sci Pollut Res 29(2):2136–2145

Jiang Q, Xie W, Han S, Wang Y, Zhang Y (2019) Enhanced adsorption of Pb(II) onto modified hydrochar by polyethyleneimine or H_3PO_4: An analysis of surface property and interface mechanism. Colloids Surf, A 583(September):123962

Kolagatla S, Subramanian P, Schechter A (2018) Nanoscale mapping of catalytic hotspots on Fe, N-modified HOPG by scanning electrochemical microscopy-atomic force microscopy. Nanoscale 10(15):6962–6970

Li Y, Han Y, Li W, Li Y, Zhang D, Lan Y (2020) Efficient removal of As(III) via simultaneous oxidation and adsorption by magnetic sulfur-doped Fe-Cu-Y trimetal oxide nanoparticles. Environ Res 180:108896

Li S, Xu H, Wang L, Ji L, Li X, Qu Z, Yan N (2021) Dual-functional sites for selective adsorption of mercury and arsenic ions in $[SnS_4]^{4-}$/MgFe-LDH from wastewater. J Hazard Mater 403:123940

Lin L, Zhang G, Liu X, Khan ZH, Qiu W, Song Z (2019) Synthesis and adsorption of Fe–Mn–La-impregnated biochar composite as an adsorbent for As(III) removal from aqueous solutions. Environ Pollut 247:128–135

Liu Z, Deng B, Li S, Zou Z (2018) Optimization of solvent-free microwave assisted extraction of essential oil from Cinnamomum camphora leaves. Ind Crops Prod 124:353–362

Luo J, Yu D, Hristovski KD, Fu K, Shen Y, Westerhoff P, Crittenden JC (2021) Critical review of advances in engineering nanomaterial adsorbents for metal removal and recovery from water: mechanism identification and engineering design. Environ Sci Technol 55(8):4287–4304

Meng A, Cheng B, Tan H, Fan J, Su C, Yu J (2021) TiO_2/polydopamine S-scheme heterojunction photocatalyst with enhanced CO_2-reduction selectivity. Appl Catal B 289:120039

Qin H, Hu T, Zhai Y, Lu N, Aliyeva J (2020) The improved methods of heavy metals removal by biosorbents: a review. Environ Pollut 258:113777

Rha S, Jo HY (2021) Waste foundry dust (WFD) as a reactive material for removing As(III) and Cr(VI) from aqueous solutions. J Hazard Mater 412:125290

Samuel M, Sarswat A, Muthukumar H, Jacob JM, Mukesh M, Pugazhendhi A (2021) Nanomaterials as adsorbents for As(III) and As(V) removal from water: a review. J Hazard Mater 424:127572

Shakoor MB, Niazi NK, Bibi I, Shahid M, Saqib ZA, Nawaz MF et al (2019) Exploring the arsenic removal potential of various biosorbents from water. Environ Int 123:567–579

Somasekhara Reddy MC, Nirmala V, Ashwini C (2017) Bengal Gram Seed Husk as an adsorbent for the removal of dye from aqueous solutions—Batch studies. Arab J Chem 10:S2554–S2566

Tabatabaiee Bafrooee AA, Moniri E, Ahmad Panahi H, Miralinaghi M, Hasani AH (2021) Ethylenediamine functionalized magnetic graphene oxide (Fe_3O_4@GO-EDA) as an efficient adsorbent in Arsenic(III) decontamination from aqueous solution. Res Chem Intermed 47(4):1397–1428

Tang Q, Shi C, Shi W, Huang X, Ye Y, Jiang W et al (2019a) Preferable phosphate removal by nano-La(III) hydroxides modified mesoporous rice husk biochars: role of the host pore structure and point of zero charge. Sci Total Environ 662:511–520

Tang Y, Li M, Mu C, Zhou J, Shi B (2019b) Ultrafast and efficient removal of anionic dyes from wastewater by polyethyleneimine-modified silica nanoparticles. Chemosphere 229:570–579

Ullah M, Nazir R, Khan M, Khan W, Shah M, Afridi SG, Zada A (2020) The effective removal of heavy metals from water by activated carbon adsorbents of Albizia lebbeck and Melia azedarach seed shells. Soil Water Res 15(1):30–37

Wang C, Luan J, Wu C (2019) Metal-organic frameworks for aquatic arsenic removal. Water Res 158:370–382

Wen T, Wang J, Yu S, Chen Z, Hayat T, Wang X (2017) Magnetic Porous Carbonaceous material produced from tea waste for efficient removal of As(V), Cr(VI), Humic acid, and Dyes. ACS Sustain Chem Eng 5(5):4371–4380

Zeng H, Wang F, Xu K, Zhang J, Li D (2020) Optimization and regeneration of chitosan-alginate hybrid adsorbent embedding iron-manganese sludge for arsenic removal. Colloids Surf A 607:125500

Zhang F, Wang X, Xionghui J, Ma L (2016) Efficient arsenate removal by magnetite-modified water hyacinth biochar. Environ Pollut 216:575–583

Zhang M, Ma X, Li J, Huang R, Guo L, Zhang X et al (2019) Enhanced removal of As(III) and As(V) from aqueous solution using ionic liquid-modified magnetic graphene oxide. Chemosphere 234:196–203

Zhang S, Zhu S, Zhang H, Liu X, Xiong Y (2020a) Synthesis and characterization of rice husk-based magnetic porous carbon by pyrolysis of pretreated rice husk with $FeCl_3$ and $ZnCl_2$. J Anal Appl Pyrol 147:104806

Zhang T, Zhao D, Wang L, Meng R, Zhao H, Zhou P et al (2020b) A facile precursor pyrolysis route to bio-carbon/ferrite porous architecture with enhanced electromagnetic wave absorption in S-band. J Alloy Compd 819:153269

Zhang R, Liu D, Wu D, Liu Y, Gui J, Zhong C et al (2021) Low Temperature Synthesis of Nitrogen-rich Biomass for High-performance Removal of Phosphate. J Environ Chem Eng 10(1):107000

Zhu N, Yan T, Qiao J, Cao H (2016) Adsorption of arsenic, phosphorus and chromium by bismuth impregnated biochar: adsorption mechanism and depleted adsorbent utilization. Chemosphere 164:32–40